SAND2005-7952C

Combined Effects of Curvature and Strain on Hydrogen Enriched Lean Methane Flames

Raymond L. Speth*, Youssef M. Marzouk† and Ahmed F. Ghoniem*

*Massachusetts Institute of Technology, Cambridge MA, 02139, USA
†Sandia National Laboratories, Livermore, CA, 94551, USA

Abstract

Hydrogen enrichment of some hydrocarbon fuels has been shown to improve lean premixed combustion stability and to extend flammability limits in a number of recent experiments. We suggest that these trends can be explained by the impact of hydrogen on the flame response to strain rate and curvature. Toward this end, we perform simulations of curved methane-hydrogen flames with detailed chemistry and transport while subjecting the flames to steady strain rates. Strong curvature, typical of turbulent conditions, is imposed on a number of flames while fixing their adiabatic burning temperature and varying their overall stoichiometry and hydrogen-to-methane ratio. Results show that adding hydrogen improves lean methane flames' response to strain rate, increasing their temperatures and burning rates at low strain rates, and delaying extinction at higher strain rates. Positive curvature reinforces the effect of hydrogen enrichment over the entire range of strain rates, further increasing the temperature and heat release rates. Both effects are consistent with preferential diffusion effects, with hydrogen reducing the effective Lewis number of the flame. This is supported by the rise in the radical concentrations within the flame, and the enlargement of the reaction zone under enrichment. Reaction pathways show that although higher strain rates lead to incomplete oxidation in all cases, hydrogen addition tends to counter this effect.

Keywords: laminar flames, hydrogen, stretched flames, curved flames

1. Introduction

Hydrogen addition has received recent attention as a method for improving the performance of lean premixed combustion systems. It is frequently desirable to operate devices such as gas turbines at relatively low flame temperatures to reduce formation of pollutants, NO_x in particular. However, low flame speeds, susceptibility to extinction, and combustion-related instabilities restrict the ability to operate near the lean flammability limit.

In the case of unstrained methane–air flames, hydrogen addition has a relatively small impact on the laminar flame speed and the lean flammability limit. For mixtures with 10% H_2, the increase in burning speed is typically 5% over a range of equivalence ratios [1]. In contrast, hydrogen enrichment has been shown to substantially increase burning velocity and to inhibit extinction in turbulent and strained environments [2, 3, 4]. This paper investigates the ef-

fects of hydrogen blending on strained, curved laminar methane–air flames by examining changes in the flame structure and reaction pathways.

The flames considered in this paper are laminar flames modified by strain rate and curvature. While the contributions of strain rate and curvature to flame stretch are well-known, curvature can exert an influence on flame structure and burning that is not captured by stretch alone [5]. The stretch of a flame surface element δA is defined [6] as

$$\kappa \equiv \frac{1}{\delta A}\frac{d\delta A}{dt} = \boldsymbol{\nabla}_t \cdot \mathbf{v}_t + (\mathbf{V}\cdot\mathbf{n})\,(\boldsymbol{\nabla}\cdot\mathbf{n}) \qquad (1)$$

where $\mathbf{v}_t$ is the flow velocity tangential to the flame surface, $\mathbf{V}$ is the velocity of the flame, and $\mathbf{n}$ is the unit normal vector of the flame surface, pointing towards the reactants. Numerous analytical studies have described the impact of stretch on premixed flames, typically using asymptotic analyses and simplified models of flame structure [7, 8, 9]. These studies yield simple expressions for the variation of burning velocity and flame temperature from their unstretched values, emphasizing the interaction of stretch with preferential diffusion (e.g., non-unity Lewis number) effects. Analytical studies of curvature coupled with stretch have shown that curvature may influence flame speed when stretch is present [10]. Numerical studies with more complete models of kinetics and transport corroborate some of these results [11], but extend them to wider regimes of stretch rate and to unsteady flow-flame interactions. In addition, detailed experimental and numerical studies of cylindrical laminar flames have described the impact of stretch and curvature on flame structure and extinction characteristics [12].

Recent experimental studies have observed a dramatic impact of hydrogen enrichment on turbulent flames that experience vigorous stretch and curvature, improving lean premixed combustion stability and extending flammability limits in a dump combustor [13]. This impact suggests important interactions among strain rate, curvature, and preferential transport in hydrogen-enriched premixed flames that we explore with a detailed physical model.

2. Modeling

The flame presented here is a laminar flame stabilized in a planar or axisymmetric stagnation flow, as depicted in Fig. 1. Reactants are supplied on the right, products are supplied on the left, and the flame stabilizes in the vicinity of the stagnation point. The potential flow velocity field for the planar case is

$$u = ax \qquad v = -ay \qquad (2)$$

where a is the time-varying strain rate parameter and x and y are the coordinates tangential and normal to the flame, respectively. The stretch rate of the planar flame, computed with Eq. 1, is simply $\kappa = a$. In the cylindrical case, the velocity field is

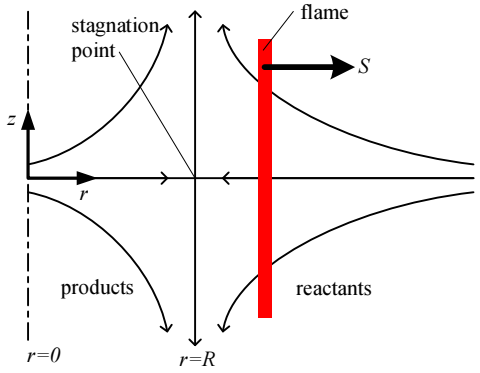

Fig. 1: Schematic of a positively curved cylindrical flame stabilized in an axisymmetric stagnation flows.

$$u = az \qquad v = \frac{a}{2}\left(\frac{R^2 - r^2}{r}\right) \qquad (3)$$

where the coordinates are as defined in Fig. 1 and R is the radius of the stagnation surface. Here the stretch rate is

$$\kappa = a + \frac{1}{R_f}\frac{dR_f}{dt} \qquad (4)$$

where R_f is the flame radius, defined as

$$R_f \equiv \frac{\int_0^\infty q'''\, r\, dr}{\int_0^\infty q'''\, dr} \qquad (5)$$

When the flame is stationary, the stretch rate reduces to $\kappa = a$ and thus curvature does not contribute to flame stretch. In this configuration, the flame is curved azimuthally and stretched axially. Direct simulations by Rutland and Trouve [14] show that cylindrical curvature predominates over spherical curvature on flame surfaces in turbulent reacting flow, and thus the stretched cylindrical flame is a useful prototype.

The flame radius is controlled by dynamically adjusting the stagnation point radius. This is in contrast to the model we presented previously [15] in which the stagnation line coincided with the centerline, allowing adjustment of the flame location only through variation of the strain rate. With the present model we may define essentially any arbitrary combination of strain rate and curvature. Additionally, this configuration permits both positively curved (convex towards the reactants) and negatively curved (convex towards the products) flames.

Governing equations for both cylindrical and Cartesian coordinates may be written simultaneously with the introduction of the parameter α, where $\alpha = 1$ for the cylindrical flame and $\alpha = 0$ for the planar flame. For the planar flame, y replaces r as the spatial coordinate. The unburned mixture density is ρ_{ub} and the axial velocity of the unburned mixture is u_{ub}. Introducing the similarity variable $U \equiv u/u_{ub}$ and the notation $V \equiv \rho v$, the momentum, continuity, species and energy equations for the flame are, respectively:

$$\rho\frac{\partial U}{\partial t} + \rho U\frac{1}{a}\frac{da}{dt} + \rho U^2 a + V\frac{\partial U}{\partial r} = \rho_{ub}\left(\frac{1}{a}\frac{da}{dt} + a\right) + \frac{1}{r^\alpha}\frac{\partial}{\partial r}\left(\mu r^\alpha \frac{\partial U}{\partial r}\right) \quad (6)$$

$$\frac{\partial \rho}{\partial t} + \rho U a + \frac{1}{r^\alpha}\frac{\partial}{\partial r}\left[r^\alpha V\right] = 0 \quad (7)$$

$$\rho\frac{\partial Y_k}{\partial t} + V\frac{\partial Y_k}{\partial r} = -\frac{1}{r^\alpha}\frac{\partial}{\partial r}\left[r^\alpha j_k\right] + \dot{\omega}_k W_k \quad (8)$$

$$\rho\frac{\partial T}{\partial t} + V\frac{\partial T}{\partial r} = \frac{1}{c_p}\left(\frac{1}{r^\alpha}\frac{\partial}{\partial r}\left[r^\alpha \lambda\frac{\partial T}{\partial r} + r^\alpha q_d\right] - \sum_k^K c_{p,k} j_k \frac{\partial T}{\partial r} - \sum_k^K h_k \dot{\omega}_k W_k\right) \quad (9)$$

The diffusion mass flux of species k is

$$j_k = -\rho D_{km}\frac{W_k}{\overline{W}}\frac{\partial X_k}{\partial r} - D_k^T\frac{1}{T}\frac{\partial T}{\partial r} \quad (10)$$

In the above equations, Y_k and X_k are respectively the mass and mole fractions for species k; W_k, $\dot{\omega}_k$ and h_k are the molecular weight, molar production rate and specific enthalpy for species k; $\overline{W}$ is the mixture molecular weight; c_p is the specific heat of the mixture; λ is the thermal conductivity; q_d is the Dufour heat flux; μ is the dynamic viscosity; D_{km} and D_k^T are the mixture averaged and thermal diffusion coefficients, respectively; the total number of species is K.

The governing equations for the flame are discretized using an implicit finite difference method. The solution is obtained using a preconditioned inexact Newton-Krylov method. CHEMKIN and TRANSPORT libraries are used to evaluate chemical source terms and the various physical properties. Details of the numerical method may be found in previous papers [16, 15, 17]. We use a modified version of the GRI-Mech 3.0 kinetic model [18], where the nitrogen chemistry has been removed to decrease computational cost.

3. Results

In this section, we present results obtained for steady planar and positively curved flames over a range of strain rates and a selection of fuel compositions. The baseline case is a methane–air flame at atmospheric pressure with equivalence ratio $\phi = 0.5$ and unburned temperature $T_u = 300$ K. We consider two variations on this baseline case, with H_2 comprising either 10% or 20% of the fuel by volume. For each hydrogen-enriched mixture, we adjust the equivalence ratio so that the burned gas temperature T_b is equal to that of the baseline case.

For positively curved flames, the flame radius is held constant at $R_f = 2.5$ mm. This radius is chosen to be comparable to the flame thickness, on the order of 1–2 mm, to highlight the effect of curvature. With each flow configuration and fuel composition, we obtained steady-state integral properties and flame structures at strain rates varying from from 10 s^{-1} to 800 s^{-1}. Direct simulations [19] and experimental diagnostics of turbulent reacting flows suggest that positively strained elements prevail over negatively (compressively) strained ones, and thus the present parameter range is representative of realistic flow-flame interactions.

3.1. Integral Properties

Figure 2 shows the integral heat release rate and maximum temperature as a function of strain rate for each flame configuration. To facilitate direct comparison of the curved and planar flames, we define a heat release rate per unit area of flame surface. For the cylindrical flame this is

$$q'' \equiv \frac{1}{R_f}\int_0^\infty q'''\, r\, dr = \int_0^\infty q'''\, dr \quad (11)$$

using the definition of R_f given in Eq. 5. For the planar flame, the equivalent heat release rate is $q'' \equiv \int_{-\infty}^{\infty} q'''\, dy$.

All six cases show the same qualitative trends with respect to strain rate. Based on the slope of each curve in Fig. 2, these trends can be divided into two regimes. At low strain rates, the heat release rate and maximum temperature immediately *rise* with increasing strain, peaking at moderate strain rates. Further increasing the strain rate then *decreases* the heat release rate, eventually reducing it below its unstrained value. The maximum temperature also decreases with strain rate at high values of the latter, falling towards the adiabatic flame temperature T_b. Because these flames are supported by a hot products stream emanating from the centerline, the maximum temperature never drops below this value. However, the heat release rate continues to decline steadily in the large-a regime; this can be seen as a prelude to extinction, as very high strain rates eventually lead to transport of material from the reaction zone before it can burn completely.

Hydrogen addition increases the heat release rate over the entire range of strain rates and for both the planar and positively-curved flames, with clear differences among the 0%, 10%, and 20%-hydrogen mixtures. But hydrogen addition also magnifies the *relative* rise in heat release rate at low strains—i.e., the difference between each peak heat release rate and its unstrained value. Hydrogen enrichment also causes each flame to reach a higher peak temperature, despite the fact that the adiabatic flame temperature is the same in all cases; this behavior indicates an important impact of hydrogen on the flame structure.

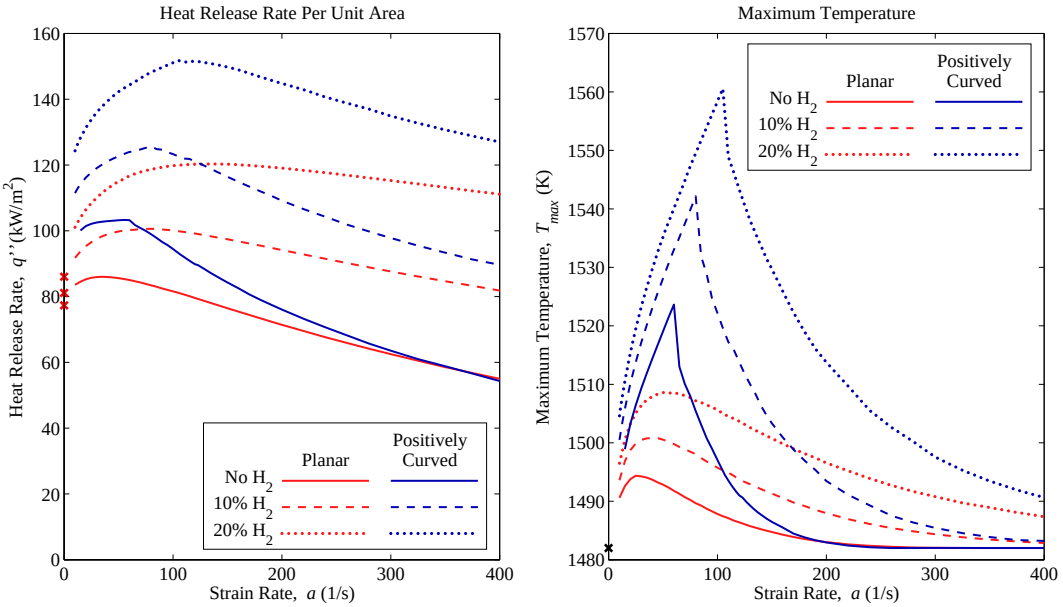

Fig. 2: Overall heat release rate (left) and maximum flame temperature (right) for curved and planar flames. The heat release rates for the planar unstrained flames (shown as $\times$ along the zero strain rate axis) are 77 $\mathrm{kW/m^2}$ for the methane-only case, 81 $\mathrm{kW/m^2}$ for the 10% H_2 case and 86 $\mathrm{kW/m^2}$ for the 20% H_2 case, determined using PREMIX with GRI-Mech 3.0. The adiabatic flame temperature for all cases is $T_b = 1482$ K.

At low and intermediate strain rates, hydrogen addition thus enhances existing trends, allowing stretch to impact the flame more strongly. This behavior is consistent with a reduction of the overall Lewis number of the enriched fuel mixtures [8], and further consistent with the higher thermal diffusivity of hydrogen, which improves its preferential flux into the products. Moreover, we find that adding hydrogen to the fuel mixture makes the flame more robust to strain, moving the strain rate at which each flame attains its peak heat release rate or peak temperature to higher values. This robustness persists at high strain rates; in this regime, Fig. 2 shows a slower decay of q'' and T_{max} with increasing strain rate in the enriched flames.

Curvature has a strong impact on the integral properties as well. Though it does not contribute to stretch in the present configuration, positive curvature strengthens the flame, particularly at low-to-intermediate values of the strain rate. Positive curvature allows a focusing of reactants and a de-focusing of heat across the flame structure. For Lewis numbers less than unity, this process should contribute to both higher heat release rates and higher temperatures within the curved flames, which we indeed observe. Sharp peaks in the maximum temperature correspond to a change in sign of the mass flux at the centerline. As the strain rate increases further, the flame thickness decreases and the effects of curvature are diminished. Planar and curved heat release rates then approach each other for each fuel mixture, as do the maximum temperatures. Unlike strain rate, however, the curvature considered here does not affect the flame in two qualitatively separate regimes (i.e., first strengthening it then weakening it). Instead, positive curvature strengthens the flame over the entire parameter range, suggesting that at high strain rates, strain and curvature may influence the flame through different mechanisms.

3.2. Flame Structure

The varied responses to strain rate, curvature, and hydrogen enrichment in Fig. 2 must reflect an impact on flame structure, and thus we examine profiles of flame temperature, heat release, and species concentrations. We compare pure methane and 20% hydrogen enriched flames in planar and positively curved configurations at strain rates of 20 $\mathrm{s^{-1}}$ and 200 $\mathrm{s^{-1}}$. To simplify comparisons, spatial profiles have been shifted by the flame location as defined in Eq. 5. For each geometry and strain rate, we plot the no-H_2 and 20%-H_2 cases together to highlight the impact of hydrogen on flame structure.

Figure 3 shows temperature and heat release rate profiles for each of these cases. In all cases, the hydrogen enriched flame exhibits more intense burning. At low to intermediate strain rates, the peak value of the heat release and the width of the reaction zone increase with strain rate. In the pure methane flame, strain rate acts in the opposite manner, reducing residence time and lowering reaction rates. The superadiabatic temperature of the hydrogen enriched flame is clearly visible at the higher strain value.

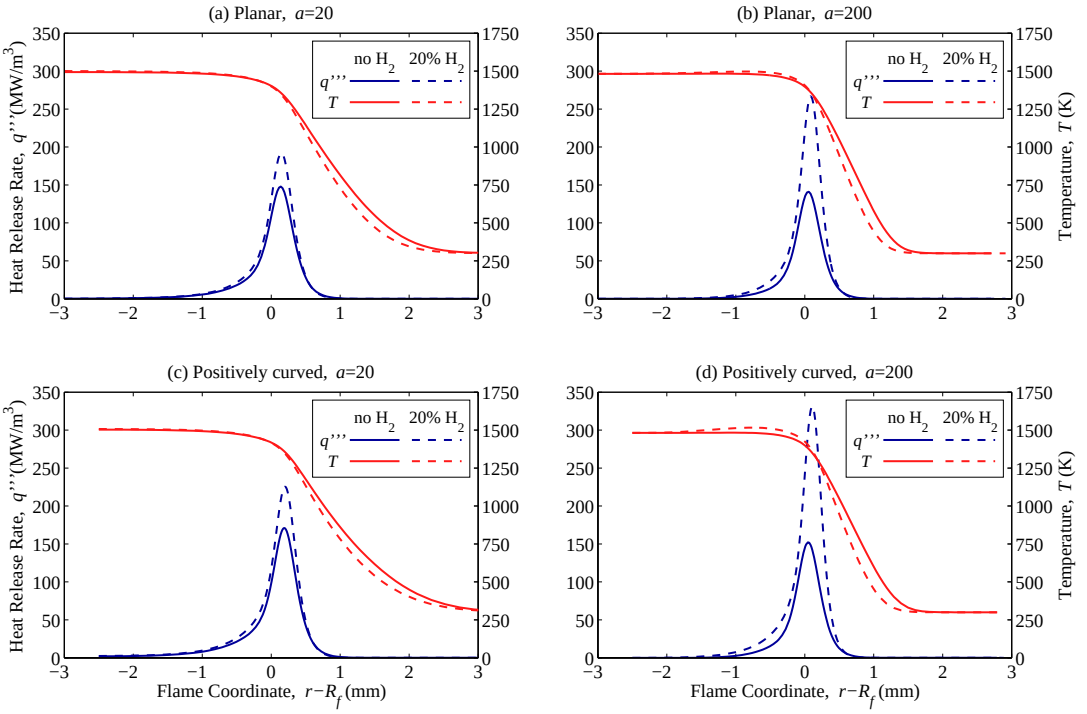

Fig. 3: Heat release and temperature profiles.

Major species profiles for the flames are shown in Fig. 4. The most noticeable effect in these profiles is the shift in product composition between the pure methane and 20% hydrogen flames, simply due to the changing stoichiometry. Gradients are noticeably steeper for the flames at higher strain, as well as for the hydrogen enhanced flames. At the higher strain rate, and especially in the 20% hydrogen flames, H_2O concentrations in excess of the equilibrium and O_2 concentrations below equilibrium are evident on the products side of the flame.

In Fig. 5 we show the profiles of the radical species O, H, and OH. The behavior of these profiles coincides with that of the heat release rate profile. Radical concentrations decrease with increasing strain for the pure methane flame, but increase in the case of the 20% hydrogen flame. For both hydrogen enriched and pure methane flames, high strain rate decreases the width of the radical profiles, especially on the products side of the flame. Curvature has a positive effect on radical concentration, as expected from the focusing of H_2 into the reaction zone.

Profiles for carbon monoxide are shown in Fig. 6. As in the radical profiles, the peak concentration of CO is more sensitive to strain rate in the pure methane flame than in the hydrogen enriched flame. In addition, these profiles show a substantial change in shape when comparing the pure methane flames with the 20% hydrogen flames. At low strain, the hydrogen enhanced flame has reduced concentrations of CO on the reactants side of the flame, but similar values in the reaction zone and on the products side. At high strain, the concentration on the reactants side is still lower for the hydrogen enriched flame, but the concentration in the reaction zone and on the products side is substantially higher, despite the lower amount of carbon in the fuel.

These profiles shown in this section demonstrate that hydrogen enrichment increases reaction zone thickness, and hence residence time. Higher radical concentrations are generated within the high temperature zone and diffuse to both sides, increasing the local reaction rates. The impact of increased radical activity is seen most vividly in Fig. 6, where CO concentrations shift toward higher temperatures with hydrogen addition. Additionally, hydrogen enrichment increases the temperature on the products side of the flame. These effects combine to improve the conversion rate of CO to CO_2, as will be shown next.

3.3. Reaction Rate Information

The impact of hydrogen enrichment on CO profiles motivates a more detailed examination of the role H_2 plays in CH_4 oxidation. We show conversion rates for the most important carbon-containing species in Fig. 7. Given a set of elementary reactions that convert species A to species B, we sum the rate-of-progress for each of these reactions and integrate this value across the flame, obtaining the total conversion rate

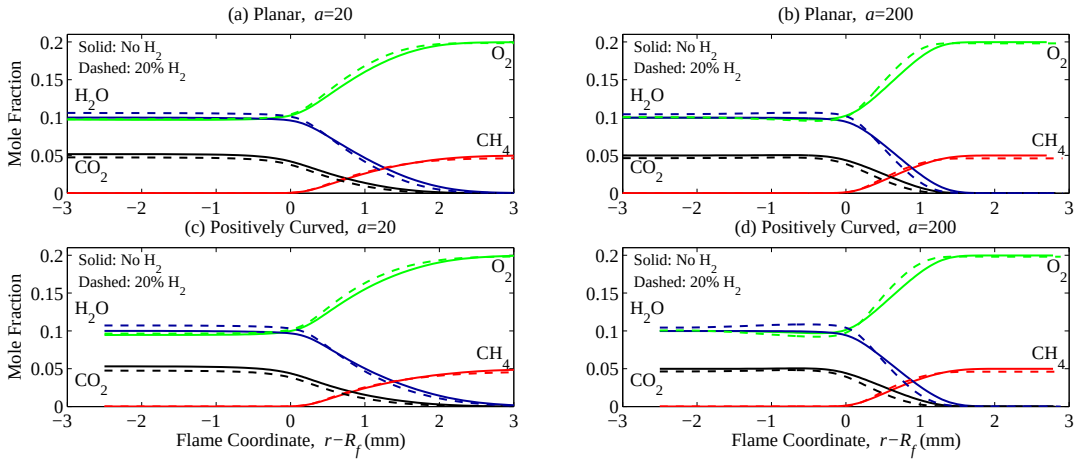

Fig. 4: Major species profiles.

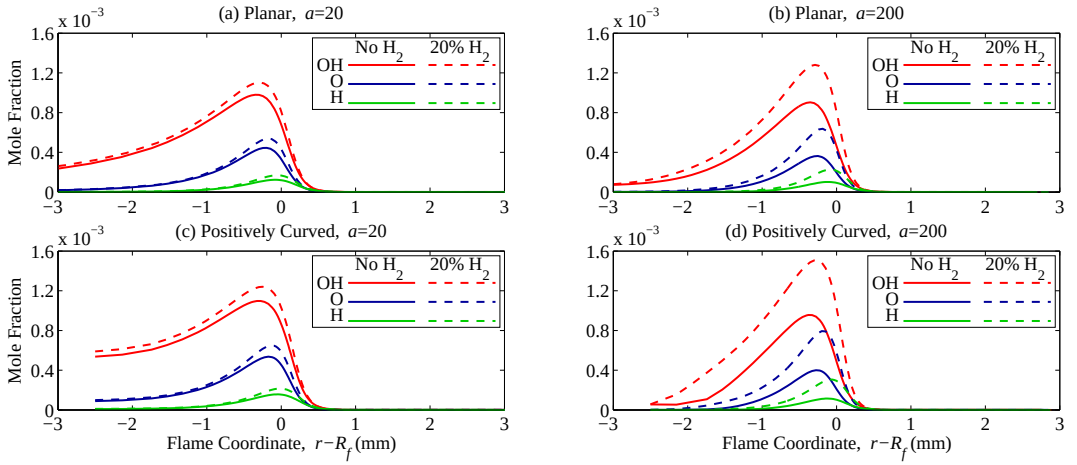

Fig. 5: Minor species profiles.

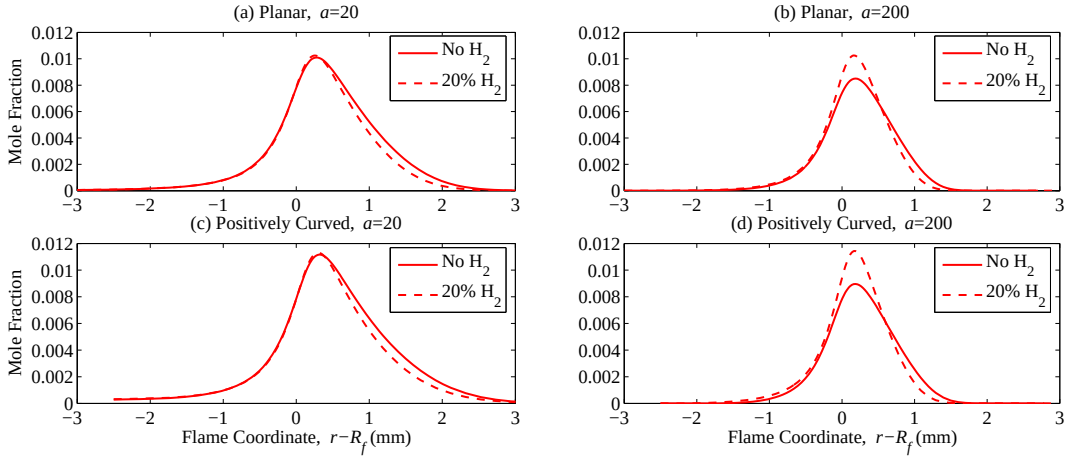

Fig. 6: Carbon monoxide profiles.

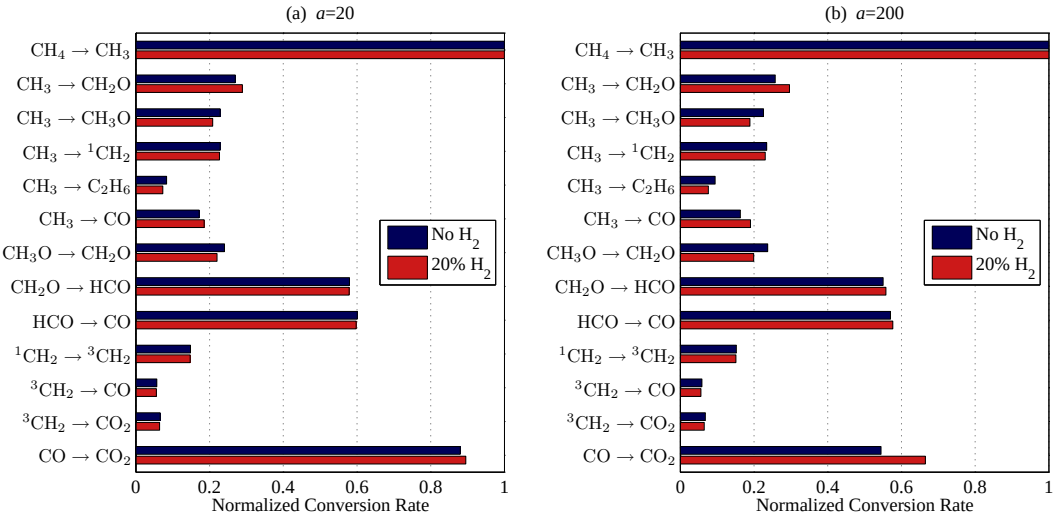

Fig. 7: Selected molar conversion rates, comparing pure methane and hydrogen enriched flames at low (a) and high (b) strain rates. Conversion rates are normalized for each flame so that the rate for $CH_4 \rightarrow CH_3$ is 1.0.

at which A is converted to B. Since the primary difference in reaction rates between cases is correlated to changes in overall burning rate, the values are normalized by the conversion rate of $CH_4 \rightarrow CH_3$ for each flame. For simplicity, we consider only the planar flame.

At low strain rate, there is very little difference between the pure methane and 20% hydrogen flames. Between the two pathways $^3CH_2 \rightarrow CO_2$ and $CO \rightarrow CO_2$, 95% of the CH_4 is ultimately converted to CO_2, in the pure methane flame, slightly more with H_2 enrichment. At higher strain rate, the conversion rate to CO_2 drops substantially, to 73% for the hydrogen enriched flame and 62% for the pure methane flame. At the same time, conversion to CO, through the pathways $CH_3 \rightarrow CO$, $HCO \rightarrow CO$ and $^3CH_2 \rightarrow CO$, is only slightly reduced by the increase in strain rate. There are a few other noticeable changes in the hydrogen enriched flame at high strain rate. More CH_3 is directly converted to CH_2O, rather than being converted to CH_3O first. Less CH_3 is converted to C_2H_6, and more is converted directly to CO. The presence of hydrogen thus alters the route by which methane is oxidized, and its effect is magnified as strain rate increases.

4. Conclusions

We have examined the combined effects of curvature and strain rate on hydrogen-enriched lean methane flames. Using a detailed numerical model in which strain rate and curvature are independent parameters, we find that curvature exerts an influence on flame structure and burning rate that cannot be captured by stretch alone.

Hydrogen addition amplifies flame response to strain rate and positive curvature. Compared to pure methane flames, hydrogen-enriched flames exhibit a stronger positive response of heat release to strain rate at low values of the strain rate, consistent with reduction of the Lewis number of the mixture. Hydrogen enrichment also renders flames more robust, shifting their peak heat release to higher strain rates and slowing their eventual decay at even stronger strains. Positive curvature further increases the heat release rate for both methane-only and hydrogen-enriched flames over a broad range of strain rates.

These behaviors are reflected in changes in the flame structure and reaction pathways. The introduction of hydrogen increases superadiabatic flame temperatures through non-unity Lewis number effects active in stretched and curved flames. Hydrogen addition also results in higher radical concentrations, a widening of the reaction zone, and shifted CO profiles, particularly at higher strain rates. These changes in flame structure alter the fuel oxidation process, increasing the amount of CH_4 that is oxidized completely and contributing to the robustness of hydrogen-enriched flames.

Acknowledgements

This work was supported by the U.S. Department of Energy, Basic Energy Sciences, MICS, under contract DE-F602-98ER25355.This work was also supported in part by an appointment to the Sandia National Laboratories Truman Fellowship in National Security Science and Engineering, sponsored by Sandia Corporation (a wholly owned subsidiary of Lockheed Martin Corporation) as Operator of Sandia National Laboratories under its U.S. Department of Energy Contract Number DE-AC04-94AL85000.

References

[1] C. Uykur, P. F. Henshaw, D. S.-K. Ting, R. M. Barron, *Int. J. Hydrogen Energy* 26 (2001) 265–273.

[2] G. S. Jackson, R. Sai, J. M. Plaia, C. M. Boggs, K. T. Kiger, *Combust. Flame* 132 (2003) 503–511.
[3] G. A. Karim, I. Wierzba, Y. Al-Alousi, *Int. J. Hydrogen Energy* 21 (7) (1996) 625–631.
[4] J. L. Gauducheau, B. Denet, G. Searby, *Combust. Sci. Technol.* 137 (1998) 81–99.
[5] T. Echekki, J. H. Ferziger, *Combust. Sci. Technol.* 90 (1993) 231–252.
[6] S. H. Chung, C. K. Law, *Combust. Flame* 55 (1984) 123–125.
[7] M. Matalon, B. J. Matkowsky, *J. Fluid Mech* 124 (1982) 239–259.
[8] C. K. Law, *Proc. Comb. Inst.* 22 (1988) 1381–1402.
[9] S. M. Candel, T. Poinsot, *Combust. Sci. Technol.* 70.
[10] D. W. Mikolaitis, *Combust. Flame* 57 (1984) 25–31.
[11] J. H. Chen, H. G. Im, *Proc. Comb. Inst.* 27 (1998) 819–826.
[12] D. M. Mosbacher, J. A. Wehrmeyer, R. W. Pitz, C. J. Sung, J. L. Byrd, *Proc. Comb. Inst.* 29 (2002) 1479–1486.
[13] A. F. Ghoniem, A. Annaswamy, S. Park, Z. C. Sobhani, *Proc. Comb. Inst.* 30 (2005) 1765–1773.
[14] C. J. Rutland, A. Trouve, *Combust. Flame* 94 (1993) 41–57.
[15] R. L. Speth, Y. M. Marzouk, A. F. Ghoniem, in: *41st Aerospace Sciences Meeting*, AIAA, 2005.
[16] Y. M. Marzouk, A. F. Ghoniem, H. N. Najm, *AIAA J.* 41 (4) (2003) 641–652.
[17] R. L. Speth, Y. M. Marzouk, A. F. Ghoniem, in: *Third MIT Conf. Comp. Fluid Solid Mech.*, 2005, pp. 867–871.
[18] G. P. Smith, D. M. Golden, M. Frenklach, N. W. Moriarty, B. Eiteneer, M. Goldenberg, C. T. Bowman, R. K. Hanson, S. Song, J. W. C. Gardiner, V. V. Lissianski, Z. Qin., *GRI-Mech 3.0*, `http://www.me.berkeley.edu/gri_mech/`.
[19] E. R. Hawkes, J. H. Chen, *Combust. Flame* 138 (2004) 242–258.